Advanced Electronic Materials

ADVANCED ELECTRONIC MATERIALS Open Access

www.advelectronicmat.de

RESEARCH ARTICLE OPEN ACCESS

Electronic Structure Effects During Cooperative Phase Transitions in Organic Semiconductor Single Crystals

Giulia Giovanelli[1] | Alessandro Lodi[1] | Mario Felipe Mery Duarte[1] | Angelo Giglia[2] | Nicola Mahne[2] | M. Alex West[3,4,5] | Josephine L. Hastings[3,4] | Yves Henri Geerts[6,7] | Michael T. Ruggiero[3,8] | Luca Catalano[3,4] | Luca Pasquali[1,2,9]

[1]Department of Engineering "Enzo Ferrari", University of Modena and Reggio Emilia, Modena, Italy | [2]CNR – Istituto Officina dei Materiali (IOM), Trieste, Italy | [3]Department of Chemistry, University of Rochester, Rochester, New York, USA | [4]Dynamic Molecular Materials Laboratory, Department of Life Sciences, University of Modena and Reggio Emilia, Modena, Italy | [5]Department of Chemistry, Reed College, Portland, Oregon, USA | [6]Laboratory of Polymer Chemistry, Université Libre de Bruxelles (ULB), Bruxelles, Belgium | [7]International Solvay Institutes, Université Libre de Bruxelles (ULB), Bruxelles, Belgium | [8]Department of Chemical and Sustainable Engineering, University of Rochester, Rochester, New York, USA | [9]Department of Physics, University of Johannesburg, Johannesburg, South Africa

Correspondence: Luca Catalano (luca.catalano@unimore.it) | Luca Pasquali (luca.pasquali@unimore.it)

Received: 3 April 2026 | **Revised:** 14 May 2026 | **Accepted:** 30 May 2026

Keywords: cooperative phase transitions | optical bandgap | organic semiconductors | polymorphism | soft x-ray reflectivity

ABSTRACT

Cooperative phase transitions in organic crystals are attracting growing interest due to their reversible, diffusionless nature, their ability to generate macroscopic dynamic phenomena, and their strong influence on the physicochemical properties of molecular materials relevant to organic electronics. Yet, the microscopic mechanisms governing these lattice- and disorder-driven transformations remain only partially understood. Because phase transitions amplify electron–phonon interactions by pushing low-frequency modes into the anharmonic regime and reorganizing molecular packing within a few kelvins, they offer a unique opportunity to directly probe lattice–electronic coupling in organic semiconductors. Here, we investigate single crystals of 2,7-di-tert-butyl-[1]benzothieno[3,2-b]benzothiophene (ditBu-BTBT), a high-performance organic semiconductor undergoing a diffusionless polymorphic transition near 70°C, to reveal how its electronic landscape, specifically the distribution of electronic states and optical bandgap, evolves across a cooperative phase transition. Variable-temperature soft x-ray reflectivity at the carbon K-edge and UV–vis absorption spectroscopy show the order–disorder transition, evidenced by energy shifts of specific resonances attributed to increased dynamics of the lateral tert-butyl groups, which become intramolecularly disordered at high temperature. Concurrently, the optical bandgap increases, reflecting reduced intermolecular interactions and band dispersion. These results directly demonstrate how cooperative polymorphic transitions modulate the electronic structure of organic semiconductors.

1 | Introduction

It has been recently established that crystalline materials characterized by a rigid, aromatic backbone (core) linked to dynamic lateral substituents [1–5] are prone to undergo solid-state polymorphic transitions in response to temperature changes, a phenomenon referred to as cooperative phase transition. This first-order process involves a reversible, diffusionless displacement of molecules within the crystal, often accompanied by minor alterations in the herringbone packing of the aromatic cores [1, 2, 6]. Because organic semiconductor performances are governed by strong electron–phonon coupling, phase transitions offer a formidable opportunity to study this complex process: as lattice modes soften, mix, or become anharmonic and symmetry

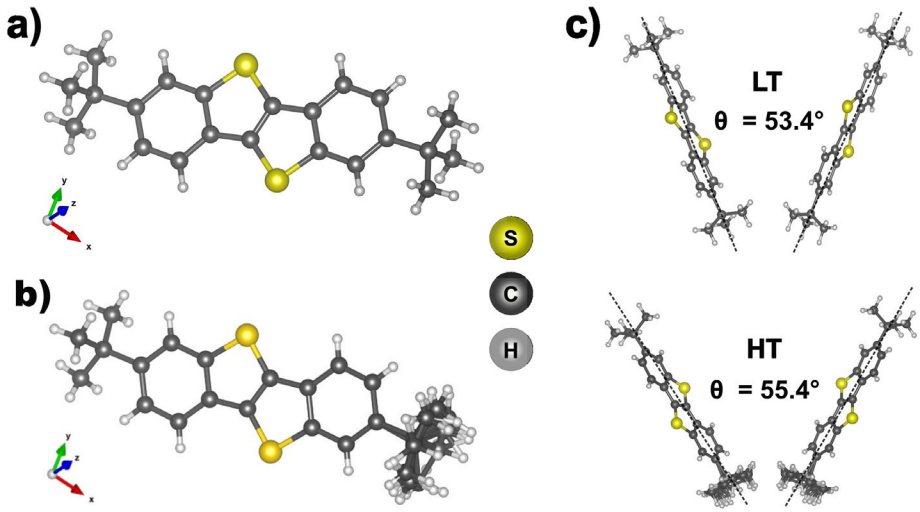

FIGURE 1 | (a) Schematic of ditBu-BTBT in the low-temperature ordered phase. (b) In the high-temperature disordered phase, the disorder is shown as a sum of three configurations of the *tert*-butyl side chain (for simplicity, this is shown for one side chain only). (c) Angle change in the herringbone pair passing from the low-temperature phase to the high-temperature phase.

changes occur, the resulting shifts in intermolecular interactions offer a rare, experimentally accessible handle to interrogate the fundamental lattice-driven mechanisms that control charge transport [7, 8]. This study focuses on ditBu-BTBT, a BTBT derivative functionalized with two bulky *tert*-butyl side groups (Figure 1a), undergoing a cooperative phase transition at ca. 70°C [6, 9].

Cooperative polymorphic transition in ditBu-BTBT single crystals has been investigated extensively using low-frequency Raman spectroscopy, x-ray diffraction (XRD), nuclear magnetic resonance (NMR) spectroscopy, Differential Scanning Calorimetry (DSC), and Polarized Optical Microscopy (POM) [1, 4–6, 9–13]. Chung et al. [6] revealed a small (~2°) dihedral angle change in the herringbone motif of the ditBu-BTBT core units, which is shown in Figure 1c. This change, although small, has been demonstrated to significantly alter the charge transfer integrals and, in principle, this can sizably affect the electronic and optical properties of the material [6]. Chung et al. [6] also concluded that the rotational motion of the *tert*-butyl side chains with increasing temperature could trigger the cooperative transition, because of the enhanced repulsive forces between adjacent side chains.

To develop a rational design of next-generation organic electronics, it is essential to understand how cooperative phase transitions influence the electronic band structure, the distribution of the electronic states, and by-extension, the optical bandgap. To investigate this, we applied variable-temperature photon-in/photon-out spectroscopic methods on ditBu-BTBT single crystals across the phase transition. Optical methods have the advantage of being non-destructive and insensitive to sample charging under irradiation with energetic photons. Specifically, we employed UV–vis absorption spectroscopy and resonant soft x-ray reflectivity (RSXRR) at the carbon K-edge. The former directly probes the optical bandgap, while the latter provides complementary evidence of both (i) the evolution of the band structure, by probing the optical transitions to empty electronic states, and (ii) the molecular arrangement and degree of order within the crystal. RSXRR has been extensively used for the characterization of organic crystalline materials and thin films [11, 14–22], exploiting the sensitivity to the rapid variation of the real and imaginary parts of the refractive index (eventually anisotropic) across the carbon K-edge, which depends strongly on the chemical and morphological properties of the system. Furthermore, since the reflectivity is defined as the ratio between the reflected signal and the incident beam, it is inherently quantitative, allowing the data to be directly compared with simulations [11, 14, 23]. RSXRR (in energy-scan mode) probes the same energy range as near edge x-ray absorption fine structure (NEXAFS), but with distinct advantages. Unlike NEXAFS, which is often limited by surface sensitivity and sample charging [24], RSXRR can access buried interfaces and bulk regions tens of nanometres below the surface. Combined with simulations of the dielectric constant, RSXRR enables a detailed characterization of sample morphology. In this work, experimental reflectivity curves as a function of photon energy at fixed grazing incidence were compared with simulations based on the Parratt formalism [25], allowing a quantitative interpretation of the structural and electronic features of the layered systems. In the present case, the crystal was treated as an aggregate of molecules. The optical constants were derived from first-principles calculation of the absorption cross-section of individual molecular building blocks.

2 | Materials and Methods

ditBu-BTBT was synthesized following a reported procedure and used for crystallization without further manipulation [9]. Single crystals were grown by slow evaporation from a 4 mg/mL solution of chloroform at room temperature, yielding plate-like crystals with lateral dimensions of 4–5 mm and thicknesses between 50 and 100 μm.

UV–vis absorption spectroscopy measurements were conducted in transmission mode, as ditBu-BTBT single crystals are transparent in the range between 380 and 750 nm. Transmission spectra

were recorded on a UV–vis spectrophotometer equipped with a deuterium lamp for the ultraviolet region, and a quartz tungsten-halogen lamp for the visible and near infrared regions (Ocean Optics, DH-2000-BAL). The sample was mounted on a copper sample holder using conductive copper tape, and the holder was fixed on a heating plate. A K-type thermocouple was positioned in close contact with the sample to monitor the temperature in real time during the acquisition of the spectra. Spectra were recorded from RT (25°C) to above 100°C, in the photon-energy range between 250 and 1000 nm. To evaluate bandgap changes, the cutoff onset in the transmission spectrum was determined by extrapolating the linear region of the absorbance curve, and the corresponding energy was taken as the optical bandgap [26–29].

Reflectivity was measured at the BEAR beamline of the Elettra synchrotron, in ultra-high-vacuum (UHV) conditions [30]. In this case, the temperature of the crystals could be varied by direct heating of the sample holder by the Joule effect, through a DC current passing in a tungsten filament. Also in this case, a K-type thermocouple was used to monitor the temperature. X-ray reflectivity across the carbon K-edge (∼280–320 eV), with a resolution of 0.1 eV, was measured by shining linearly polarized light on the sample at a grazing incidence of $\theta_{gr} = 3°$, a geometry chosen to obtain a sizable intensity of the reflected beam, which guarantees a high signal-to-noise ratio. A photodiode (IRD AXUV photodiode) mounted on the BEAR reflectometer arm was used to measure the intensities of both the direct and reflected beams. Measurements were performed in both s- and p-polarizations, although only s-polarization data are reported, as the spectra obtained in p-polarization did not offer further insight beyond that provided by the s-polarization spectra.

UV–vis and RSXRR measurements were repeated on different sample replicas to confirm observations.

Reflectivity was simulated adopting the Parratt's formalism [25], a recursive, dynamical method for calculating x-ray reflectivity from layered structures, treating the crystal as a continuous homogeneous medium with optical constants derived from the scattering cross section of the single molecule [11, 14, 23]. Due to the alternating herringbone orientation of the ditBu-BTBT molecules in the crystal, we treated the system as isotropic to simplify calculations – i.e., optical constants were evaluated considering, on average, isotropic angular orientations of the molecular units. This approach is reasonable, since experimentally we did not observe any angular effects on the reflectivity line-shape, i.e., by varying light incidence from s- to p- polarization, which are usually related to the presence of strong anisotropies.

The real and imaginary parts of the refractive index were derived starting from the Density Functional Theory (DFT) calculation of the absorption cross section of the single molecule [11] using the StoBe code [31]. The atomic geometry of the ditBu-BTBT molecule was taken from the single-crystal structure obtained via x-ray diffraction [9]. The ground-state molecular orbitals were calculated using the revised Perdew–Burke–Ernzerhof (RPBE) exchange/correlation functional and triple zeta valence polarization (TZVP) atomic basis sets [31, 32]. Absorption spectra in correspondence to the carbon K-edge for all nonequivalent carbon atoms were calculated with the transition-potential method [32]. The spectra from the various atomic centres were ultimately merged, after applying a ΔKohn–Sham correction, to achieve alignment on the energy scale [33, 34]. The optical constants were obtained considering the crystal as an aggregate of non-interacting molecules.

3 | Results and Discussion

Reflectivity spectra recorded at the carbon K-edge (Figure 2) exhibit characteristic π^* and σ^* features. The region between 284 and 287 eV corresponds to C1s → π^* transitions within the conjugated molecular core. The higher-energy structures are attributed to C1s → σ^* transitions, involving both the core and the lateral alkyl chains. The features in the experimental spectra were first assigned based on literature [35–38], and then validated through molecular calculations (see below).

Two main effects associated with the temperature variation are observed. First, there is a progressive reduction of the overall intensity, which we attribute to an increased diffuse scattering caused by the formation of cracks and defects in the crystal during the increase of the temperature, which could be clearly observed by the naked eye (Figure S9) [39]. The incoming photon beam is at a grazing incidence of 3° with respect to the crystal plane; this results in a large beam footprint (ca. 2 mm), which averages over a relatively large portion on the sample, encompassing multiple cracks and defects that develop as the temperature increases. The second effect is related to the displacement of the centroid of the broad structure associated to C1s → σ^* transitions, around 305–310 eV. The structure exhibits a broadening as the temperature passes from RT to above 100°C; this is interpreted in terms of increased vibrational effects with temperature. Remarkably, a sudden shift to lower energies of about 1 eV is also observed when passing across the phase-transition temperature. To elucidate the specific nature of the molecular levels involved in this effect in more detail, first-principles simulations of the absorption cross section of the molecules in the crystal were carried out. These were then used to simulate the reflectivity line-shape. Calculated absorption cross sections are shown in Figure 3a, where the total cross section is presented together with the isolated contributions of the carbons in the BTBT core and in the side chains. Following a previously reported method [11], the absorption cross section at the C K-edge was used to evaluate the imaginary part of the molecular scattering factor (f_2), and then, through the use of Kramers-Kronig transformations, the real part (f_1). Using the molecular density, derived from crystallographic data reported in the literature [9], the real and imaginary parts of the refractive index, n and k, were finally obtained (Figures S7 and S8). Reflectivity simulations were carried out using the Parratt formalism [25], a recursive method based on the Fresnel equations, considering the experimental grazing incidence of 3°.

Figure 3b presents the comparison between the simulated and the experimental reflectivity at RT. Despite the DFT simulation being performed on a single molecule, the agreement between experiment and theory is remarkable. The calculation provides a parameter-free molecular reference based on DFT absorption cross sections of the isolated molecule, from which the crystal's optical constants are constructed, therefore perfect agreement with experiment is not expected, given the neglect of intermolecular and solid-state effects. Despite this, it is remarkable that (i)

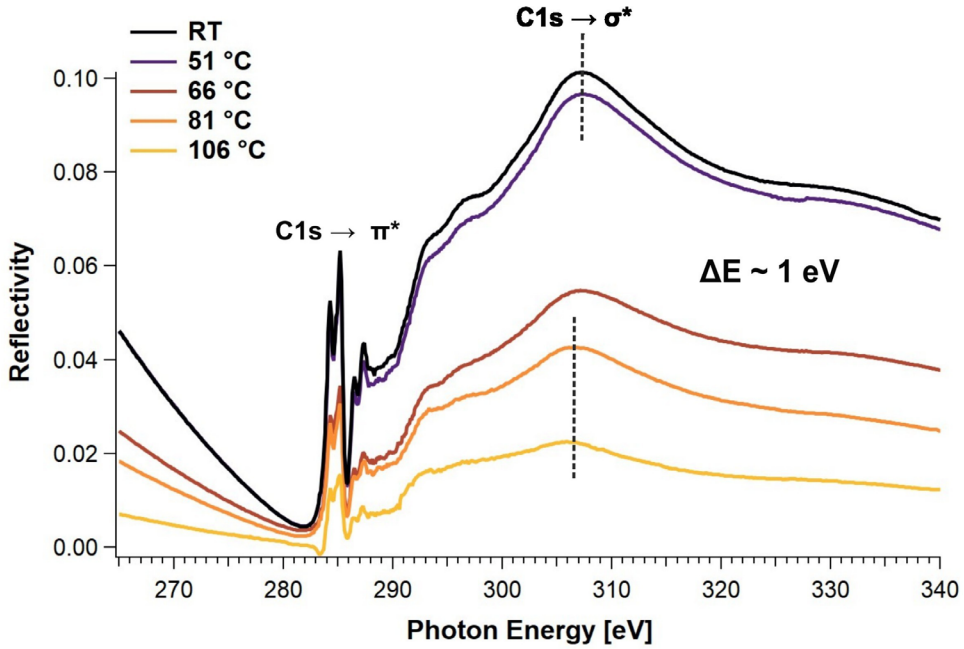

FIGURE 2 | Reflectivity experimental spectra at the carbon K-edge, recorded from RT to 106°C. At increasing temperature, two main effects are observed: a progressive decrease of the reflected intensity, and a shift of approximately $\Delta E \approx 1$ eV associated with the maximum of the C1s → σ* transitions.

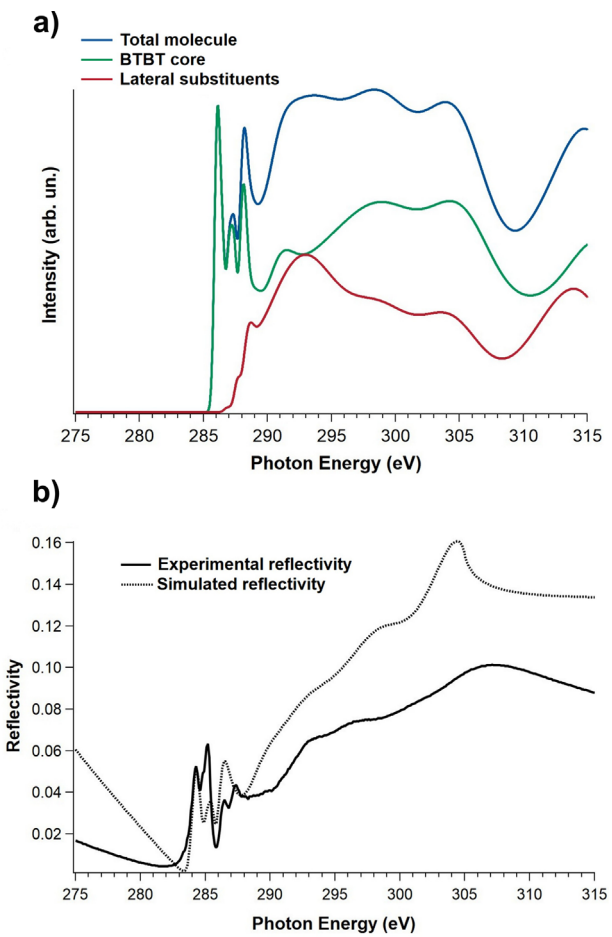

FIGURE 3 | (a) Calculated absorption cross sections arising from the core, the lateral substituents and the entire molecule. (b) Comparison between the simulated and experimental reflectivity.

the simulation reproduces quantitatively the overall intensity and (ii) the main features observed experimentally are captured by the simulation, allowing for a precise assignment of the different spectral weights. Specifically, the simulation reproduces the main π* and σ* transitions. Spectral oscillations around 285 eV are related to π* transitions originating from the conjugated carbons in the molecular core, while the high-energy structures above 290 eV, arising from σ* transitions, are partially associated with the carbons in the lateral *tert*-butyl chains, with maxima at about 293, 304–305 and 310–315 eV and partially to atoms in the BTBT core (see simulations of the absorption cross sections along the different molecular axes in Figures S2–S5).

Based on our simulations and on the reported observations [6] on the role of the *tert*-butyl side chains in the transition, we associate the σ* peak shift to carbons in these terminal units, especially to the features that simulations show at 310–315 eV. We ascribe the shift to the increased structural disorder within the molecule, as the system passes from the low-temperature ordered phase to the high-temperature "disordered" phase. This structural transition likely causes bond distortions (i.e., slight elongation) and rearrangement in the chains, thereby resulting in a reduction in the excitation energy associated with the transition. This experimental behavior supports the interpretation that structural disorder inside the molecule, in the lateral chains, plays a key role in driving the cooperative transition [6]. Moreover, σ* transitions in organic compounds are highly sensitive to the local order and shifts associated with bond reorganization have been observed several times in thin-film systems [22, 24].

The structural disorder inside the molecule, which becomes particularly significant when the phase transition occurs, leads to a weakening of the intermolecular interactions between neighboring ditBu-BTBT molecules. This interpretation is consistent with Raman data [1, 32], showing a sudden redshift and

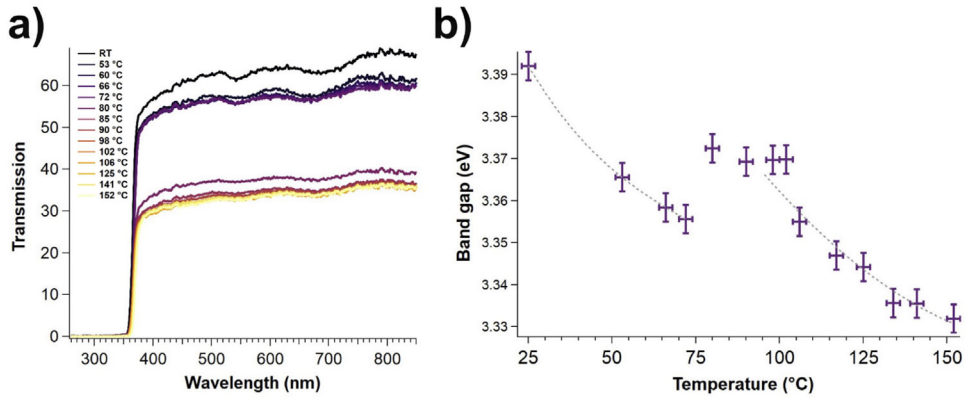

FIGURE 4 | (a) UV–vis spectra of a ditBu-BTBT single crystal recorded in transmission mode. The spectra were taken while heating the crystal through a heating plate. (b) Optical bandgap as a function of temperature for a ditBu-BTBT single crystal. The dotted lines are only a guide for the eye and do not represent fits.

broadening of the entire Raman spectrum at the transition, coherent with substantially diminished intermolecular forces that cannot be explained solely by thermal effects. Crossing the phase-transition temperature drives the system toward reduced crystallinity, contributing to the observed shift of the σ^* structure (Figure 2) [40–45]. This is also consistent with structural analysis showing variations in the crystalline arrangement [6] (Figure 1c).

Concerning the bandgap, the transmission spectra in the UV–vis range are shown in Figure 4a. The ditBu-BTBT single crystal shows complete transparency in the visible and IR ranges, while featuring strong absorption between 250 and 350 nm, in the near-UV, due to $\pi \rightarrow \pi^*$transitions. It can be noticed that, as the temperature increases during the measurement, the overall intensity decreases, in consistency with the increased scattering determined by the progressive formation of defects and cracks, as already observed in the reflectivity spectra. The sharp change in transmission consistently occurs around the transition temperature, indicating that while defects may form throughout the heating process, their proliferation is enhanced at the phase transition, when the system undergoes a structural reorganization. The transmission onset is associated with the optical bandgap. This is evaluated by linear extrapolation on the absorbance [26], as shown in Figure S6.

The temperature dependence of the optical bandgap is shown in Figure 4b. As expected for conventional semiconductors, the progressive heating shows a general decrease of the bandgap with increasing temperature. This behavior is typically attributed to enhanced vibrational motion and increased structural disorder within the molecules as the system evolves from RT to higher temperature. Remarkably, this trend is interrupted by a sudden increase in the correspondence of the phase transition. At temperatures approaching ~100°C, the bandgap begins to decrease again. As the system transitions from the low to the high temperature phase, the resulting structural reorganization – involving less ordered molecular configurations with respect to RT—induces weaker intermolecular interactions, leading to a wider optical bandgap [46]. A comparable bandgap increase has also been reported in hybrid perovskite semiconductors, where phase transitions introduce enhanced structural disorder and reduced band dispersion, ultimately weakening solid-state effects due to the loss of long-range atomic order [47–50].

4 | Conclusions

The presented combined experimental and theoretical investigation reveals that the cooperative phase transition in ditBu-BTBT single crystals has a clear impact on the electronic properties. Our results establish phase transitions as a sensitive regime in which lattice dynamics and packing reorganizations manifest directly in the electronic structure, providing a valuable platform for advancing phonon-engineering strategies in organic semiconductors [7]. On one hand, reflectivity shows that the transition involves an intramolecular reorganization, with a relaxation of the bond lengths between C atoms in the lateral chains of the molecular building blocks. This is attributed to an increased disorder within the molecules, associated with the configuration of the *tert*-butyl side groups. Therefore, the phase transition induces not only collective structural changes but also localized variations of the electronic states at the molecular level. Previous structural studies showing that the system evolves above the transition into a less ordered conformation, accompanied by reduced intermolecular interactions, support our interpretation. On the other hand, UV–vis spectra show a small but sizable increase of the optical bandgap at the transition temperature. This is related to an intermolecular effect, i.e., the reduction of the solid-state interactions associated with the increased level of disorder in the crystal, as probed by structural analyses. These findings demonstrate that phase transitions in amphidynamic molecular crystals can induce considerable variations of the electronic structure, with potential implications for organic electronics, especially in applications requiring tunable or responsive materials, in contexts where structure-function relationships are critical. Although our measurements were performed on single crystals, the insights gained provide a useful framework to interpret the behavior observed in thin films, which are more relevant for device fabrication and more sensitive to molecular packing. The cooperative phase transition likely contributes to the reduction of solid-state coupling in thin films, leading to smaller transfer integrals and, consequently, lower charge carrier mobility, as previously reported [6]. Notably, OFETs based on ditBu-BTBT

thin films not only retain this cooperative phase transition but also exploit it to achieve a functional memory effect, enabling reversible and tunable modulation of charge carrier mobility within transistors [6]. A deeper understanding of cooperative phase transitions in organic systems and their influence on the electronic behavior of thin-film devices is therefore crucial for the design of next-generation smart, multifunctional materials with controllable electronic responses.

Acknowledgements

The experiments were carried out at the BEAR beamline at Elettra (proposal 20240135). This research was funded by the European Commission under the HORIZON-MSCA-2023-PF-01 project CHIMERA, ID 101151367, and the Italian MUR under PRIN 2022 Project 'PETRA', Project n. 2022T7ZSEK—CUP E53D23001860006, in the frame of Next Generation EU, Mission 4, Component 1. MTR, AW, JH, and LC thank the National Science Foundation (OISE-2420126 and DMR-2348765) for financial support. L.C. thanks the University of Modena and Reggio Emilia for financial support.

Open access publishing facilitated by Universita degli Studi di Modena e Reggio Emilia, as part of the Wiley - CRUI-CARE agreement.

Conflicts of Interest

The authors declare no conflicts of interest.

Data Availability Statement

The data that support the findings of this study are available from the corresponding author upon reasonable request.

References

1. M. Asher, M. Bardini, L. Catalano, et al., "Mechanistic View on the Order–Disorder Phase Transition in Amphidynamic Crystals," *The Journal of Physical Chemistry Letters* 14 (2023): 1570–1577, https://doi.org/10.1021/acs.jpclett.2c03316.

2. M. A. Garcia-Garibay, "Crystalline Molecular Machines: Encoding Supramolecular Dynamics into Molecular Structure," *Proceedings of the National Academy of Sciences* 102 (2005): 10771–10776, https://doi.org/10.1073/pnas.0502816102.

3. X. Wang, W. Wang, C. Yang, D. Han, H. Fan, and J. Zhang, "Thermal Transport in Organic Semiconductors," *Journal of Applied Physics* 130 (2021): 170902, https://doi.org/10.1063/5.0062074.

4. L. Catalano and P. Naumov, "Exploiting Rotational Motion in Molecular Crystals," *CrystEngComm* 20 (2018): 5872–5883, https://doi.org/10.1039/c8ce00420j.

5. L. Catalano, R. Sharma, D. P. Karothu, et al., "Toward on-Demand Polymorphic Transitions of Organic Crystals via Side Chain and Lattice Dynamics Engineering," *Journal of the American Chemical Society* 146 (2024): 31911–31919, https://doi.org/10.1021/jacs.4c11289.

6. H. Chung, D. Dudenko, F. Zhang, et al., "Rotator Side Chains Trigger Cooperative Transition for Shape and Function Memory Effect in Organic Semiconductors," *Nature Communications* 9 (2018): 1–12, https://doi.org/10.1038/s41467-017-02607-9.

7. B. M. T. C. Peluzo, R. Meena, L. Catalano, G. Schweicher, and M. T. Ruggiero, "Exploring the Interplay of Lattice Dynamics and Charge Transport in Organic Semiconductors: Progress toward Rational Phonon Engineering," *Angewandte Chemie International Edition* 64 (2025): 202507566, https://doi.org/10.1002/anie.202507566.

8. Y. Tsutsui, G. Schweicher, B. Chattopadhyay, et al., "Unraveling Unprecedented Charge Carrier Mobility through Structure Property Relationship of Four Isomers of Didodecyl[1]Benzothieno[3,2- b][1]Benzothiophene," *Advanced Materials* 28 (2016): 7106–7114, https://doi.org/10.1002/adma.201601285.

9. G. Schweicher, V. Lemaur, C. Niebel, et al., "Bulky End-Capped [1]Benzothieno[3,2- b]Benzothiophenes: Reaching High-Mobility Organic Semiconductors by Fine Tuning of the Crystalline Solid-State Order," *Advanced Materials* 27 (2015): 3066–3072, https://doi.org/10.1002/adma.201500322.

10. H. Ebata, T. Izawa, E. Miyazaki, et al., "Highly Soluble [1]Benzothieno[3,2-b]Benzothiophene (BTBT) Derivatives for High-Performance, Solution-Processed Organic Field-Effect Transistors," *Journal of the American Chemical Society* 129 (2007): 15732–15733, https://doi.org/10.1021/ja074841i.

11. L. Pasquali, N. Mahne, A. Giglia, et al., "Analysis of Resonant Soft X-Ray Reflectivity of Anisotropic Layered Materials," *Surfaces* 4 (2021): 18–30, https://doi.org/10.3390/surfaces4010004.

12. H. Sirringhaus, "25th Anniversary Article: Organic Field-Effect Transistors: the Path beyond Amorphous Silicon," *Advanced Materials* 26 (2014): 1319–1335, https://doi.org/10.1002/adma.201304346.

13. M. Pope and C. E. Swenberg, *Electronic Processes in Organic Crystals and Polymers* (Oxford University Press, 1999), https://doi.org/10.1093/oso/9780195129632.001.0001.

14. R. Capelli, E. Da Como, G. Kociok-Köhn, C. Fontanesi, A. Verna, and L. Pasquali, "Quantitative Resonant Soft X-Ray Reflectivity from an Organic Semiconductor Single Crystal," *The Journal of Chemical Physics* 150 (2019): 094707, https://doi.org/10.1063/1.5080800.

15. M. Nayak and G. S. Lodha, "Optical Response near the Soft X-Ray Absorption Edges and Structural Studies of Low Optical Contrast System Using Soft X-Ray Resonant Reflectivity," *Journal of Atomic, Molecular, and Optical Physics* 2011 (2011): 1–23, https://doi.org/10.1155/2011/649153.

16. J. H. Carpenter, A. Hunt, and H. Ade, "Characterizing Morphology in Organic Systems with Resonant Soft X-Ray Scattering," *Journal of Electron Spectroscopy and Related Phenomena* 200 (2015): 2–14, https://doi.org/10.1016/j.elspec.2015.05.006.

17. C. Wang, A. Garcia, H. Yan, et al., "Interfacial Widths of Conjugated Polymer Bilayers," *Journal of the American Chemical Society* 131 (2009): 12538–12539, https://doi.org/10.1021/ja905293m.

18. H. Ade, "Characterization of Organic Thin Films with Resonant Soft X-Ray Scattering and Reflectivity near the Carbon and Fluorine Absorption Edges," *The European Physical Journal Special Topics* 208 (2012): 305–318, https://doi.org/10.1140/epjst/e2012-01626-y.

19. W. Ma, B. Vodungbo, K. Nilles, P. Theato, and J. Lüning, "Surface and Bulk Ordering in Thin Films of a Symmetrical Diblock Copolymer," *Journal of Polymer Science Part B: Polymer Physics* 51 (2013): 1282–1287, https://doi.org/10.1002/polb.23335.

20. J. Als-Nielsen and D. McMorrow, *Elements of Modern X-ray Physics* (Wiley, 2011).

21. D. Atwood, *Soft X-Rays and Extreme Ultraviolet Radiation* (Cambridge University Press, 1999).

22. L. Pasquali, S. Mukherjee, F. Terzi, et al., "Structural and Electronic Properties of Anisotropic Ultrathin Organic Films from Dichroic Resonant Soft X-Ray Reflectivity," *Physical Review B* 89 (2014): 045401, https://doi.org/10.1103/PhysRevB.89.045401.

23. R. Capelli, N. Mahne, K. Koshmak, et al., "Quantitative Resonant Soft X-Ray Reflectivity of Ultrathin Anisotropic Organic Layers: Simulation and Experiment of PTCDA on Au," *The Journal of Chemical Physics* 145 (2016): 024201, https://doi.org/10.1063/1.4956452.

24. J. Stöhr, C. Noguera, and T. Kendeleiwicz, "Auger and Photoelectron Contributions to the Electron-Yield Surface Extended X-Ray-Absorption Fine-Structure Signal," *Physical Review B* 30 (1984): 5571–5579, https://doi.org/10.1103/PhysRevB.30.5571.

25. L. G. Parratt, "Surface Studies of Solids by Total Reflection of X-Rays," *Physical Review* 95 (1954): 359–369, https://doi.org/10.1103/PhysRev.95.359.

26. J. C. S. Costa, R. J. S. Taveira, C. F. R. A. C. Lima, A. Mendes, and L. M. N. B. F. Santos, "Optical Band Gaps of Organic Semiconductor Materials," *Optical Materials* 58 (2016): 51–60, https://doi.org/10.1016/j.optmat.2016.03.041.

27. A. B. Murphy, "Band-Gap Determination from Diffuse Reflectance Measurements of Semiconductor Films, and Application to Photoelectrochemical Water-Splitting," *Solar Energy Materials and Solar Cells* 91 (2007): 1326–1337, https://doi.org/10.1016/j.solmat.2007.05.005.

28. A. S. Bhadwal, R. M. Tripathi, R. K. Gupta, N. Kumar, R. P. Singh, and A. Shrivastav, "Biogenic Synthesis and Photocatalytic Activity of CdS Nanoparticles," *RSC Advances* 4 (2014): 9484–9490, https://doi.org/10.1039/c3ra46221h.

29. N. Ghobadi, "Band Gap Determination Using Absorption Spectrum Fitting Procedure," *International Nano Letters* 3 (2013): 1–4, https://doi.org/10.1186/2228-5326-3-2.

30. S. Nannarone, F. Borgatti, A. Deluisa, et al., "The BEAR Beamline at Elettra," *AIP Conference Proceedings* 705 (2004): 450–453, https://doi.org/10.1063/1.1757831.

31. K. Hermann, L. G. M. Pettersson, and M. E. Casida, *StoBe-deMon (Version 3.0) and Documentation for STOBE2007* (StoBe Software, 2007).

32. L. Triguero, L. G. M. Pettersson, and H. Ågren, "Calculations of Near-Edge X-Ray-Absorption Spectra of Gas-Phase and Chemisorbed Molecules by Means of Density-Functional and Transition-Potential Theory," *Physical Review B* 58 (1998): 8097–8110, https://doi.org/10.1103/PhysRevB.58.8097.

33. C. Kolczewski, R. Püttner, O. Plashkevych, et al., "Detailed Study of Pyridine at the C1 s and N1 s Ionization Thresholds: the Influence of the Vibrational Fine Structure," *The Journal of Chemical Physics* 115 (2001): 6426–6437, https://doi.org/10.1063/1.1397797.

34. M. Cavalleri, M. Odelius, D. Nordlund, A. Nilsson, and L. G. M. Pettersson, "Half or Full Core Hole in Density Functional Theory X-Ray Absorption Spectrum Calculations of Water?," *Physical Chemistry Chemical Physics* 7 (2005): 2854–2858, https://doi.org/10.1039/b505723j.

35. A. Schoell, Y. Zou, D. Huebner, et al., "A Comparison of Fine Structures in High-Resolution X-Ray-Absorption Spectra of Various Condensed Organic Molecules," *The Journal of Chemical Physics* 123 (2005): 044509, https://doi.org/10.1063/1.1978872.

36. J. Taborski, P. Väterlein, H. Dietz, U. Zimmermann, and E. Umbach, "NEXAFS Investigations on Ordered Adsorbate Layers of Large Aromatic Molecules," *Journal of Electron Spectroscopy and Related Phenomena* 75 (1995): 129–147, https://doi.org/10.1016/0368-2048(95)02397-6.

37. Y. Zou, L. Kilian, A. Schöll, T. Schmidt, R. Fink, and E. Umbach, "Chemical Bonding of PTCDA on Ag Surfaces and the Formation of Interface States," *Surface Science* 600 (2006): 1240–1251, https://doi.org/10.1016/j.susc.2005.12.050.

38. J. B. Gustafsson, E. Moons, S. M. Widstrand, M. Gurnett, and L. S. O. Johansson, "Thin PTCDA Films on Si(001): 2. Electronic Structure," *Surface Science* 572 (2004): 32–42, https://doi.org/10.1016/j.susc.2004.08.030.

39. The cracks may also result from the necessity of securing the sample with clips during the measurement.

40. S. D. Perera, S. Shokatian, J. Wang, and S. G. Urquhart, "Temperature Dependence in the NEXAFS Spectra of n-Alkanes," *The Journal of Physical Chemistry A* 122 (2018): 9512–9517, https://doi.org/10.1021/acs.jpca.8b10713.

41. A. Schöll, R. Fink, E. Umbach, G. E. Mitchell, S. G. Urquhart, and H. Ade, "Towards a Detailed Understanding of the NEXAFS Spectra of Bulk Polyethylene Copolymers and Related Alkanes," *Chemical Physics Letters* 370 (2003): 834–841, https://doi.org/10.1016/S0009-2614(03)00215-X.

42. T. Fransson, Y. Harada, N. Kosugi, et al., "X-Ray and Electron Spectroscopy of Water," *Chemical Reviews* 116 (2016): 7551–7569, https://doi.org/10.1021/acs.chemrev.5b00672.

43. M. Johnson, T. Hawly, B. Zhao, M. Halik, A. Nefedov, and R. Fink, "Field-Induced Modification of the Electronic Structure in BTBT-Based Organic Thin Films Observed by NEXAFS Spectroscopy," *Applied Physics Letters* 121 (2022): 183503, https://doi.org/10.1063/5.0105893.

44. H. Watanuki, K. Mitsuhara, and M. Takizawa, "Molecular Orientation Analysis of a C₈-BTBT Thin Film Grown under an External Temperature Gradient," *e-Journal of Surface Science and Nanotechnology* 16 (2018): 79–83, https://doi.org/10.1380/ejssnt.2018.79.

45. J. Kikuma and B. P. Tonner, "XANES Spectra of a Variety of Widely Used Organic Polymers at the C K-Edge," *Journal of Electron Spectroscopy and Related Phenomena* 82 (1996): 53–60, https://doi.org/10.1016/S0368-2048(96)03049-6.

46. S. Refaely-Abramson, S. Sharifzadeh, M. Jain, R. Baer, J. B. Neaton, and L. Kronik, "Gap Renormalization of Molecular Crystals from Density-Functional Theory," *Physical Review B* 88 (2013): 081204, https://doi.org/10.1103/PhysRevB.88.081204.

47. C. M. M. Soe, C. C. Stoumpos, M. Kepenekian, et al., "New Type of 2D Perovskites with Alternating Cations in the Interlayer Space, $(C(NH_2)_3)(CH_3NH_3)_nPb_nI_{3n+1}$: Structure, Properties, and Photovoltaic Performance," *Journal of the American Chemical Society* 139 (2017): 16297–16309, https://doi.org/10.1021/jacs.7b09096.

48. M. Mączka, M. Ptak, A. Gągor, D. Stefańska, and A. Sieradzki, "Layered Lead Iodide of [Methylhydrazinium]$_2PbI_4$ with a Reduced Band Gap: Thermochromic Luminescence and Switchable Dielectric Properties Triggered by Structural Phase Transitions," *Chemistry of Materials* 31 (2019): 8563–8575, https://doi.org/10.1021/acs.chemmater.9b03775.

49. X. Ren, X. Yan, A. S. Ahmad, et al., "Pressure-Induced Phase Transition and Band Gap Engineering in Propylammonium Lead Bromide Perovskite," *The Journal of Physical Chemistry C* 123 (2019): 15204–15208, https://doi.org/10.1021/acs.jpcc.9b02854.

50. Y. J. Cao, L. Zhou, L. He, P. P. Shi, Q. Ye, and D. W. Fu, "Phase Transition and Band Gap Regulation by Halogen Substituents on the Organic Cation in Organic–Inorganic Hybrid Perovskite Semiconductors," *Chemistry—A European Journal* 26 (2020): 14124–14129, https://doi.org/10.1002/chem.202001266.

Supporting Information

Additional supporting information can be found online in the Supporting Information section.

Supporting File: aelm70457-sup-0001-SuppMat.docx.